EXPERIENCES WITH POINT-MASS GRAVITY FIELD MODELLING IN THE PERTH REGION, WESTERN AUSTRALIA

S. J. Claessens[1], **W. E. Featherstone**[2], **F. Barthelmes**[3]

1. Department of Physical, Geometrical and Space Geodesy, Faculty of Civil Engineering and Geosciences, Delft University of Technology, Thijsseweg 11, 2629 JA Delft, The Netherlands, e-mail: s.j.claessens@student.tudelft.nl, Tel: +31 15 278 4169, Fax: +31 15 278 3711

2. Geodesy Group, Department of Spatial Sciences, Curtin University of Technology, GPO Box U1987, Perth, WA 6845, Australia, e-mail: W.Featherstone@curtin.edu.au, Tel: +61 8 9266 2218, Fax: +61 8 9266 2703

3. GeoForschungsZentrum, Telegrafenberg, D-14473 Potsdam, Germany, e-mail: bar@gfz-potsdam.de, Tel: +49 331 288 1143, Fax: +49 331 288 1169

ABSTRACT

Gravimetric geoid modelling in the Perth region of Western Australia has attracted much attention in recent years because of the numerous restrictions in this area, such as the presence of the Darling Fault system and variable gravity data coverage and quality. This paper presents the results of experiments to determine the effectiveness of free-positioned point-mass modelling in relation to the previous attempts based on Stokes's integral. It is shown that the point-mass modelling technique does not yield improved fits to 99 local GPS-levelling data with a standard deviation of the fit of $\pm$17.5cm. However, the experiments do show that the technique is a useful tool for conveniently identifying areas where there are large topographic mass density contrasts and mismatches among the gravity data used. Therefore, the technique, though apparently not optimal for geoid modelling in this region at this point in time, may provide a useful indicator of problems that will affect geoid computations using other techniques.

INTRODUCTION

The Perth region of Western Australia provides a challenging 'field laboratory' for gravimetric geoid determination and modelling. This is due to its geographical location close to the Australian coast and the perturbations of the Earth's gravity field and topography caused by the near-linear Darling Fault (Figure 1). The geological structure of the Darling Fault is explained in some detail elsewhere (eg. Dentith *et al.*, 1993, Middleton *et al.*, 1993, Friedlieb *et al.*, 1997; Featherstone, 2000), so will not be duplicated here. It is interesting to note that, from a Dutch perspective, Vening Meinesz (1948) was the first to observe the large gravity anomaly over the Darling Fault. Incredibly, from only two measurements (one at the University of Western Australia and another on the Yilgarn Block), he deduced a geological model that is very similar to models presented today (eg. Lambeck, 1987; Dentith *et al.*,1993).

The relevant characteristics are a (free-air) gravity anomaly of $\sim$100mGal over $\sim$15km (Figure 1), a topographic mass-density change of over 500kgm^{-3}, a variation in topographic elevation from 0m to $\sim$400m on the Australian Height Datum (Figure 1), and a variety of gravity observation types (land, shipboard, altimeter) with a heterogeneous spatial coverage (Figure 2).

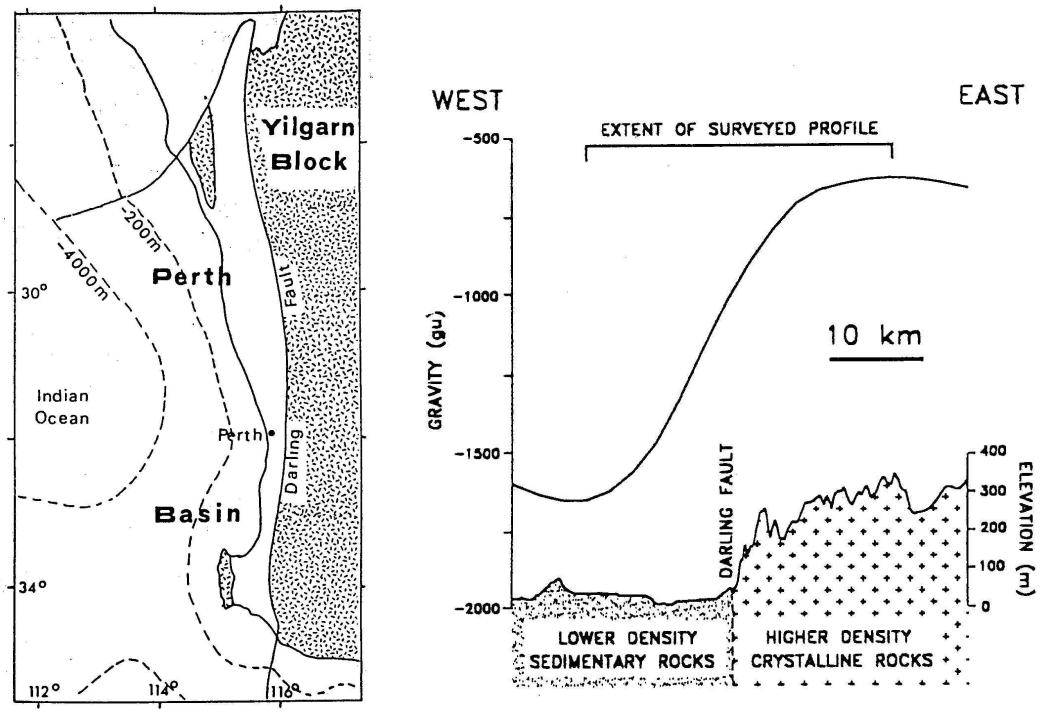

Fig. 1. Schematic map of the Darling Fault (from Lambeck, 1987) and cross section over the Perth region (from Friedlieb *et al.* 1997) showing a Bouguer gravity profile.

The above factors have compounded to make gravimetric geoid modelling based on Stokes's integral quite problematic. The AUSGeoid98 gravimetric geoid model of Australia (Johnston and Featherstone, 1998; Featherstone *et al.*, 2001), while an improvement on AUSGeoid93 (Steed and Holtznagel, 1994) in this region, is not sufficiently accurate for the routine replacement of spirit levelling by GPS techniques. A pragmatic, interim solution to height transformation in this region was achieved by combining AUSGeoid98 with GPS-AHD heights using least-squares collocation (Featherstone, 2000). A more recent investigation by Tziavos and Featherstone (2001) uses a simplistic topographic mass-density model. This improved the results upon the gravimetric AUSGeoid98, but only after a bias and tilt fit to local GPS-levelling data.

This paper describes the results of several experiments to determine if a point-mass modelling technique provides a superior alternative to the above techniques based on Stokes's integral. It was originally anticipated that this approach could be used to identify systematic errors in the Australian Height Datum (AHD), but as will be seen, problems with the spatial coverage and quality of the gravity data in this region prevented this. Instead, it will be shown that the free-positioned point-mass modelling technique (eg. Barthelmes and Kautzleben, 1983; Barthelmes, 1986; Barthelmes, 1989; Barthelmes and Dietrich, 1991; Barthelmes et al., 1991) is a useful tool for the identification of large contrasts in topographic mass-density and inconsistencies or errors in the gravity data.

The concept of point-mass modelling for geoid determination is quite straightforward. It relies on the principle of superposition of a number of either fixed- or free-positioned point masses with varying magnitude that generate an external gravitational potential and acceleration. This is achieved simply by the application of Newton's laws of gravitation, in which the potential (V) is given by

$$V = \frac{Gm}{l} \tag{1}$$

and the gravitational acceleration (g) is given by

$$g = \frac{Gm}{l^2} \tag{2}$$

where G is the Newtonian gravitational constant, m is the magnitude of the point mass and l is the direct distance between the computation point and the point mass. The magnitude, position and number of point masses situated inside the Earth are optimised so that their superposition generates gravity acceleration (equation 2) at the Earth's surface, which is consistent with gravity observations. These exact same point masses are then used to generate the gravitational potential (equation 1) and thence the geoid. As with gravimetric geoid computation based on Stokes's integral, the resulting geoid heights can be compared with GPS-levelling data to validate the effectiveness of the technique. However, this is subject to errors in the GPS and levelling data.

Point-mass modelling has been used in gravity field determination for over 35 years. Barthelmes (1986) attributes the first study to Weightman (1965). Over the years, two classes of point-mass modelling have been utilised.

1. Fixed-positioned point-mass modelling, where a regular grid of point masses is used inside the Earth to generate the external gravity field (eg. Vermeer, 1995). The advantage of this approach is that it linearises and simplifies the computation because only the magnitudes, and not the positions, of the point masses have to be determined by inversion. An example of the application of this technique to geoid modelling is the computation of a German quasigeoid (Ihde et al., 1998).
2. Free-positioned point-mass modelling, where both the magnitudes and the positions of the point masses inside the Earth are determined simultaneously by inversion. This presents a non-linear problem, which must be solved iteratively and with several constraints. Examples of the application of this technique to global geoid modelling are given in Barthelmes and Dietrich (1991) and Barthelmes *et al.* (1991), and to regional geoid studies in the Gulf of Bothnia (Lehmann, 1993).

On the basis of the data available for this investigation (described later), there are two different reasons to use the free-positioned point-mass technique:

1. Free-positioned point-mass techniques adapt the distribution of the point masses to the geological situation, i.e. more point masses are placed in areas with highly varying mass-densities. The Darling Fault in the Perth region consists of a large density variation of over 500kgm^{-3}, which can possibly better be modelled with a free-positioned point-mass model.
2. Free-positioned point-mass techniques do not need to use a regular grid of gravity data, while grid-based fixed-positioned methods do (Vermeer, 1998). The use of a grid of gravity data was not desirable in this study, because the gravity data was not homogeneously distributed over the whole area and because there are some large data gaps (Figure 2). The errors that occur in a gridding or prediction process are avoided.

THE FREE-POSITIONED POINT-MASS METHOD OF BARTHELMES

In geodesy, the use of observations related to the gravity field of the Earth to predict unobserved gravity field quantities is known as the inverse problem (eg. Lehmann, 1993). A narrower definition is given in Heiskanen and Moritz (1967): the inverse problem is the determination of the mass distribution inside the Earth from the potential. According to Stokes's theorem, there are infinitely many mass distributions which generate a single harmonic function as the potential exterior to the gravitating masses. This is the well-known problem of non-uniqueness in the inversion of potential field data. Therefore, additional information is necessary. This can be furnished by density models of the Earth's interior that can be obtained by seismic measurements and by making assumptions about the density structure that minimise numerical effort or simplify the mathematical relationships. Nevertheless, the problem of non-uniqueness will always remain.

The simplest assumption is that the density distribution of the Earth can be described by a finite number of point masses that are placed under the Earth's surface. In practice, these point masses are actually spherically symmetric mass disturbances that can either be positive or negative with respect to some arbitrary reference mass. Although this contravenes Newton's law, the resulting effect is equivalent to using all positive masses (i.e. the difference between the negative mass and the reference mass is never negative). The point masses are positioned in such a way that they generate a gravitational acceleration that fits the gravity anomalies that are computed from gravity measurements.

From equation (2), one point mass m_i at position q_i in the three-dimensional Euclidian space E^3 ($q_i \in E^3$) gives the following disturbing potential T at point P ($P \neq q_i$):

$$T(P, m_i, q_i) = T_i(P) = G m_i \phi(P, q_i) \tag{3}$$

where $\phi_i(P)$ is the base function:

$$\phi_i(P) = \phi(P, q_i) = l^{-1}(P, q_i) \tag{4}$$

By superposition of all the disturbing potentials from n point masses, the disturbing potential can be found by:

$$T(P) = \sum_{i=1}^{n} T_i(P) = G \sum_{i=1}^{n} m_i \phi_i(P) \tag{5}$$

From the total disturbing potential in equation (5), the geoid height can be computed via Bruns's equation by dividing the disturbing potential by normal gravity (γ) at the ellipsoid:

$$N(P) = \frac{T(P)}{\gamma} \tag{6}$$

The main difficulty of this technique is to construct the geometry and magnitudes of the point masses in an optimal way from observed gravity measurements (i.e. the inversion). If the real field is produced by a finite number of point masses, this problem has a unique solution, contrary to the problem for continuous mass distributions (Stromeyer and Ballani, 1984). Defining an algorithm that gives this unique solution is, however, not straightforward and is possibly numerically difficult to solve (Barthelmes, 1986).

A lot of research on free-positioned point-mass modelling has been published by what is now called the GFZ (GeoForschungsZentrum) in Potsdam, Germany (eg. Barthelmes and Kautzleben, 1983; Barthelmes, 1986; Barthelmes *et al.*, 1991; Lehmann, 1993; Lehmann, 1994). The method used in this project was developed by Barthelmes (1986). In his method, the positions of the point masses can be determined in an optimal agreement with the observed distribution of the gravity anomalies (Barthelmes and Kautzleben, 1983). However, the fundamental observation equations are

non-linear and need to be solved by iteration with some constraints. An accurate iterative solution is only possible if the base vectors that are used to represent the potential field of the point masses are nearly orthogonal. This allows the point masses to be determined sequentially, and in each step of the iteration, only the point masses in the neighbourhood of a new point need to be optimised.

Formulation of the algorithm for general base vectors in Hilbert space

The gravity field is usually observed at the Earth's surface and needs to be approximated by point masses within the Earth. An important feature in finding an algorithm to achieve this is the linear independence of the base vectors of a finite number of point masses, which is proven for point masses on a closed surface within the Earth in Kupradze and Aleksidze (1964) and for point masses with an arbitrary distribution in Stromeyer and Ballani (1984). This means that when the external gravity field produced by a finite number of point masses is known, the positions of the masses are uniquely determined. In the approximation of the real gravity field, the positions and magnitudes of the point masses should minimise the differences between the observed gravity field and the field that is formed by superposition of the point mass potentials or accelerations, while accounting for observational and other errors.

As the number of point masses used will be in the order of several hundred, finding the magnitudes and positions of these masses that minimise the differences best is a complicated task. The global minimum needs to be found, but the correct initial values for the iteration to find that minimum are lacking. Also, because the numerical accuracy of the computation is limited, it is possible that different point-mass configurations approximate the given field equally well, which makes the problem even more difficult. As stated, this is because of non-uniqueness in potential field inversion. From a practical point of view, it is therefore sufficient only to find a local minimum from whatever initial values are available; the accuracy of the solution can be increased by adding more point masses.

A norm can be defined in such a way that the local minimum will be found, which has the smallest maximum difference between the Earth's disturbing potential and the disturbing potential generated by the point masses. Barthelmes (1986) states that the local minimum that is found in this way will also be the global minimum in many cases, or will at least give a similar difference. The problem of finding this local minimum will now be formalised mathematically.

A finite number, n, of orthonormal base vectors h_i must be searched for from the set of orthonormal base vectors in a Hilbert space H $\{h_i \, \epsilon \, H, i = 1, 2, ...\}$ that approximate the Earth's disturbing potential the best. This can be formulated as:

$$\|T - \sum_{l=1}^{n} \langle T, h_{i_l} \rangle h_{i_l}\| = \min\{\|T - \sum_{l=1}^{n} \langle T, h_{k_l} \rangle h_{k_l}\| \quad | \quad k_l \, \epsilon \, N_Z\} \tag{7}$$

where $\|\cdot\|$ is the norm operator, $\langle\cdot\rangle$ is the inner product operator, T is the vector of the disturbing potential in the infinite-dimensional Hilbert space and h_i is the set of orthonormal base vectors.

Inserting the norm $\|U\| = \langle U, U\rangle^{\frac{1}{2}}$, where U is an arbitrary element, into equation (7) gives

$$\|T - \sum_{l=1}^{n} \langle T, h_{i_l}\rangle h_{i_l}\|^2 = \min\{\langle T, T\rangle - \sum_{l=1}^{n} \langle T, h_{k_l}\rangle^2 \quad | \quad k_l \,\epsilon\, N_Z\} \tag{8}$$

The left-hand-side of equation (8) is always positive, and thus the result of the difference in the right-hand-side must also be positive. Therefore the base vectors h_{i_l} can be determined by

$$\sum_{l=1}^{n} \langle T, h_{i_l}\rangle^2 = \max\{\sum_{l=1}^{n} \langle T, h_{k_l}\rangle^2 \quad | \quad k_l \,\epsilon\, N_Z\} \tag{9}$$

Equation (9) means that from the set of base vectors, the vector which has the largest inner product with vector T should be chosen in every step of an iterative approximation procedure. If $(n-1)$ base vectors have already been computed and the new base vector should be in the complete set $\{h_i, i = 1, 2, ...\}$, then this new base vector can be computed from

$$\langle T, h_{i_n}\rangle^2 = \max\{\langle T - \sum_{l=1}^{n-1} \langle T, h_{i_l}\rangle h_{i_l}, h_{k_n}\rangle^2 \quad | \quad k_n \,\epsilon\, N_Z\} \tag{10}$$

Formulation of the algorithm for point mass base vectors

Applying the above concept to the three-dimensional Euclidian space E^3, the base vectors in equation (4) need to be searched for. The positions of the point masses need to be within the Earth, i.e. q_i is within the complete three-dimensional Euclidian space E^3 except for the space outside the Earth $\overline{\Omega}$ ($q_i \,\epsilon\, E^3 \backslash \overline{\Omega}$). The following approximation algorithm can now be formulated for the free-positioned point masses. In order to achieve this, use is made of normalised base vectors, Φ_i, and coefficients, μ_i, which are given by

$$\Phi_i = \frac{\phi_i}{\|\phi_i\|} \qquad \text{and} \qquad \mu_i = G m_i \|\phi_i\| \tag{11}$$

Because the positions of all the point masses should actually be recomputed in each step of the iteration (i.e. the position and the base vectors of the i-th point mass needs to be optimised when a new point mass is added), the position also depends on the number of point masses that are computed in the previous k steps. The upper index in the following brief notation indicates this:

$$\Phi_i^k = \Phi(P, q_i^k) \qquad \text{and} \qquad \Phi^* = \Phi(P, q^*) \tag{12}$$

Equations (7) to (10) can be used after a definition of the inner product is implemented. In the first step, the position and the magnitude of the first mass is based solely on the gravity field, whereas in the next steps, the influence of the already computed point masses is subtracted from the observed

gravity field to determine the initial values for the position and magnitude of the new point mass (point b in the n-th step). In all but the first step the positions of the point masses are then optimised (point c in the n-th step). Equation (16) in point c will have to be solved iteratively. The concept of the iterative procedure is summarised as follows:

First step

Determination of q_1^1 (and Φ_1^1) and μ_1^1 by:

$$\langle T, \Phi_1^1 \rangle^2 = \max\{\langle T, \Phi^* \rangle^2 \quad | \quad q^* \, \epsilon \, E^3 \backslash \overline{\Omega}\} \qquad \text{and} \qquad \mu_1^1 = \langle T, \Phi_1^1 \rangle \tag{13}$$

n-th step

a. Determination of the approximate values $\tilde{q}_i^n$ (and $\tilde{\Phi}_i^n$) $(i = 1, ..., n-1)$ by:

$$\tilde{q}_i^n = q_i^{n-1} \qquad \text{and} \qquad \tilde{\Phi}_i^n = \Phi_i^{n-1} \tag{14}$$

b. Determination of the approximate value $\tilde{q}_n^n$ (and $\tilde{\Phi}_n^n$) by:

$$\langle T - \sum_{i=1}^{n-1} \mu_i^{n-1} \Phi_i^{n-1}, \tilde{\Phi}_n^n \rangle^2 = \max\{\langle T - \sum_{i=1}^{n-1} \mu_i^{n-1} \Phi_i^{n-1}, \Phi^* \rangle^2 \quad | \quad q^* \, \epsilon \, E^3 \backslash \overline{\Omega}\} \tag{15}$$

c. Determination of q_i^n (and Φ_i^n) and μ_i^n $(i = 1, ..., n)$ by:

$$\| T - \sum_{i=1}^{n-1} \mu_i^n \Phi_i^n \| = \min\{\| T - \sum_{i=1}^{n-1} \mu_i^* \Phi_i^* \| \quad | \quad q^* \, \epsilon \, E^3 \backslash \overline{\Omega};\ \mu_i^* \, \epsilon \, E,\ (i = 1, ..., n)\} \tag{16}$$

Practical realisation of the algorithm

In order to adopt Barthelmes's method for point-mass modelling, the main difficulty that remains is that the base vectors in Hilbert space are not orthogonal (Barthelmes, 1986). This means that in every iteration, strictly speaking, the $(n-1)$ positions and magnitudes of all point masses from the previous iterations should be recomputed. However, the influence on these $(n-1)$ point masses will not be very large, so the former positions can be used as initial values in the iteration. Another problem is to find the initial position and magnitude for the new point mass. In the orthogonal case, equation (10) can be used to find the point mass that has the largest inner product with the disturbing potential of the gravity field from the measurements. Given the above, if the base vectors were orthogonal, equation (10) could be used only once and there would be no need to recompute all the positions of the former point masses.

The linear independence of the base vectors is not dependent on the definition of the inner product, so it can be chosen somewhat arbitrarily, as long as the properties of an inner product are fulfilled.

Barthelmes (1986) has investigated the orthogonality of the base vectors of the point masses for two inner product definitions. Although complete orthogonality can never be accomplished, Barthelmes (1986) shows that the inner product

$$\langle \phi_i, \phi_j \rangle = \frac{1}{4\pi} \int_\sigma \nabla \phi_i \cdot \nabla \phi_j d\sigma \tag{17}$$

leads to base vectors that are "nearly" orthogonal when the point masses are relatively shallow and not too close together. It will be shown later that the angles between the base vectors of the point masses in Hilbert space are larger than 89° in more than 80% of the point mass combinations in the Perth region.

Determination of the initial values for the iteration

It is now possible to insert equation (17) in the algorithm (equations 14 to 16). Point b in the n-th step (equation 15) gives the initial values for the iterative optimisation in point c, which becomes:

$$[\int_\sigma \nabla \delta T_{n-1} \cdot \nabla \tilde{\Phi}_n^n d\sigma]^2 = \max\{[\int_\sigma \nabla \delta T_{n-1} \cdot \nabla \tilde{\Phi}^* d\sigma]^2 \ \mid \ q^* \ \epsilon \ E^3 \backslash \overline{\Omega}\} \tag{18}$$

where δT_{n-1} is the difference between the Earth's observed disturbing potential (T) and the disturbing potential according to the point masses (T_{PM}) computed in the earlier ($n-1$) steps:

$$\delta T_{n-1} = T - T_{PM} \qquad \text{with} \qquad T_{PM} = \sum_{i=1}^{n-1} \mu_i^{n-1} \Phi_i^{n-1} \tag{19}$$

The disturbing potential δT_{n-1} can be either positive or negative with respect to some normal gravity field, so there are areas where the vectors $\nabla \delta T_{n-1}$ point inside the Earth and there are areas where they point outside the Earth.

The square of the integral on the left-hand-side of equation (18) will become large if the new point mass is under a position with a large positive or negative value in the vector field $\nabla \delta T_{n-1}$. An approximate solution for equation (18) is therefore to place the new point mass directly underneath the position with the largest value of $|\nabla \delta T_{n-1}|$. The initial depth (D_0) for the new point mass must still be chosen, but this is not problematic. An initial depth of, for instance, 5km will generally be a good choice. If the initial depth for the new point mass is too deep, then it may be incorrectly positioned in an adjecent large positive or negative value in the vector field. Therefore, the search for the point P_{max} with the largest value for $|\nabla \delta T_{n-1}(P)|$ is now numerically very easy to solve by:

$$|\nabla \delta T_{n-1}(P_{max})| = \max\{|\nabla \delta T_{n-1}(P_i)| \ \mid \ i \ \epsilon \ \{1, ..., m\}\} \tag{20}$$

where m is the number of available surface gravity measurements.

In general, the gravity measurements will have been used to compute gravity anomalies (Δg) or, less frequently, gravity disturbances (δg) instead of disturbing potentials. In the case of gravity anomalies, P_{max} can be found by:

$$|\delta \Delta g_{n-1}(P_{max})| = \max\{|\Delta g_{n-1}(P_i)| \quad | \quad i \, \epsilon \, \{1, ..., m\}\} \tag{21}$$

where $\delta \Delta g_{n-1}$ is the difference between the observed (and computed) gravity anomalies and the gravity anomalies generated by the point masses (Δg_{PM}):

$$\delta \Delta g_{n-1} = \Delta g - \Delta g_{PM} \tag{22}$$

In equation (22), Δg_{PM} can be computed with the use of a slightly modified version of the *fundamental equation of physical geodesy* (Barthelmes, 1989):

$$\Delta g_{PM} = -\frac{\partial T_{PM}}{\partial H} + \frac{1}{\gamma}\frac{\partial \gamma}{\partial H} T_{PM} \approx \langle \frac{\boldsymbol{\gamma}}{\|\gamma\|} \, , \, \nabla T_{PM} \rangle + \frac{1}{\gamma}\frac{\partial \gamma}{\partial H} T_{PM} \tag{23}$$

where $\frac{\boldsymbol{\gamma}}{\|\gamma\|}$ gives the direction of the normal gravity unit vector with:

$$\boldsymbol{\gamma} = (\gamma_x \quad \gamma_y \quad \gamma_z)^T \tag{24}$$

and where the derivatives with respect to the orthometric height (H) can be evaluated at the geoid. The initial position for the new point-mass position is now given by:

$$\tilde{q}_n^n = \tilde{q}_n^n (R = R_{P_{max}} - D_0 \, , \, \lambda = \lambda_{P_{max}} \, , \, \varphi = \varphi_{P_{max}}) \tag{25}$$

Optimising the magnitudes of the point masses for fixed positions

After the computation of the initial position of each new point mass, the magnitude should be optimised next. Inserting the definition of the inner product (equation 17) into point c of the iterative algorithm (equation 16) gives:

$$\begin{aligned} &\int_\sigma [\nabla T(P) - \sum_{j=1}^{n} \mu_j \nabla \phi(P, q_j)]^2 d\sigma(P) \\ &= \min\{\int_\sigma [\nabla T(P) - \sum_{j=1}^{n} \mu_j^* \nabla \phi(P, q_j)]^2 d\sigma(P) \quad | \quad \mu_j^* \, \epsilon \, E \, , \, (j = 1, ..., n)\} \end{aligned} \tag{26}$$

The gravity field that needs to be approximated is only given by discrete measurements. Therefore, the integral in equation (26) can be replaced by the summation:

$$\sum_{i=1}^{m} (\boldsymbol{a}_i - \sum_{j=1}^{n} \mu_j \boldsymbol{f}_{ij})^2 = \min\{\sum_{i=1}^{m} (\boldsymbol{a}_i - \sum_{j=1}^{n} \mu_j^* \boldsymbol{f}_{ij})^2 \quad | \quad \mu_j^* \, \epsilon \, E \, , \, (j = 1, ..., n)\} \tag{27}$$

where the following abbreviations are used:

$$\boldsymbol{a}_i = (a_{xi} \quad a_{yi} \quad a_{zi})^T = \nabla T(P_i) \ , \ (i = 1, ..., m) \tag{28}$$

and

$$\boldsymbol{f}_{ij} = (f_{xij} \quad f_{yij} \quad f_{zij})^T = \nabla \Phi(P_i, q_j) \ , \ (i = 1, ..., m \, , \, j = 1, ..., n) \tag{29}$$

and where in geocentric Cartesian coordinates {x, y, z}

$$P_i = (P_{xi} \quad P_{yi} \quad P_{zi})^T \qquad \text{and} \qquad q_j = (q_{xj} \quad q_{yj} \quad q_{zj})^T \tag{30}$$

In general, the gradient of the disturbing potential (∇T) that is needed in equation (28) will, however, not be known. Most of the time, only gravity anomalies will be available. In this case, $\boldsymbol{a}_i$ will become a scalar:

$$a_i = \Delta g(P_i) \ , \ (i = 1, ..., m) \tag{31}$$

It can now be seen that the fundamental equation of geodesy (equation 23) for a point mass becomes:

$$\Delta g_{PM} = \sum_{j=1}^{n} \Big(\frac{\gamma_x}{\gamma} \mu_j \Phi_x(P_i, q_j) + \frac{\gamma_y}{\gamma} \mu_j \Phi_y(P_i, q_j) + \frac{\gamma_z}{\gamma} \mu_j \Phi_z(P_i, q_j) + \frac{1}{\gamma} \frac{\partial \gamma}{\partial H} \mu_j \Phi(P_i, q_j) \Big) \tag{32}$$

with

$$\Phi_s(P_i, q_j) = \frac{\partial \Phi}{\partial P_{si}} \qquad , \qquad s \, \epsilon \, \{x, y, z\} \tag{33}$$

where s can either be x, y or z. The vector $\boldsymbol{f}_{ij}$ will now also become a scalar. From equation (32), and inserting equation (4) the scalar f_{ij} can be computed in geocentric Cartesian coordinates {x, y, z} by:

$$f_{ij} = \frac{\gamma_x}{\gamma} \frac{q_{xj} - P_{xi}}{l^3(P_i, q_j)} + \frac{\gamma_y}{\gamma} \frac{q_{yj} - P_{yi}}{l^3(P_i, q_j)} + \frac{\gamma_z}{\gamma} \frac{q_{zj} - P_{zi}}{l^3(P_i, q_j)} + \frac{1}{\gamma} \frac{\partial \gamma}{\partial H} \frac{1}{l(P_i, q_j)} \tag{34}$$

Equation (27) can now be solved using a least-squares adjustment, if the number of point masses n is smaller than the number of measurements m. In this case, the system that needs to be solved has the form $\boldsymbol{y} = A\boldsymbol{x}$:

$$\begin{bmatrix} a_1 \\ a_2 \\ \vdots \\ a_m \end{bmatrix} = \begin{bmatrix} f_{11} & f_{12} & \cdots & f_{1n} \\ f_{21} & f_{22} & \cdots & f_{2n} \\ \vdots & \vdots & \ddots & \vdots \\ f_{m1} & f_{m2} & \cdots & f_{mn} \end{bmatrix} \begin{bmatrix} \mu_1 \\ \mu_2 \\ \vdots \\ \mu_N \end{bmatrix} \tag{35}$$

The well-known (unweighted) least-squares solution for the system in equation (35) is now easy to compute by:

$$\hat{\boldsymbol{x}} = (A^T A)^{-1} A^T \boldsymbol{y} \tag{36}$$

which gives estimates for the masses in fixed positions.

Optimising the positions of the point masses

The fixed-positioned solution, derived in the previous section, can now be extended to the free-positioned case. If not only the magnitudes, but also the positions of the point masses need to be optimised, the problem becomes non-linear. In the method of Barthelmes (1986), the linearisation method of Newton-Kantorovych is used (Bronstein and Semendyayev, 1983). In this method, use is made of a linearised Taylor expansion. When using gravity anomalies for point mass modelling, equation (32) must be linearised, which leads to:

$$a_i = \tilde{a}_i + \sum_{j=1}^{n} \left(g_{ij} \Delta\mu_j + g_{xij} \Delta q_{xj} + g_{yij} \Delta q_{yij} + g_{zij} \Delta q_{zij} \right) \tag{37}$$

with

$$g_{ij} = \frac{\gamma_x}{\gamma} \Phi_x(P_i, \tilde{q}_j) + \frac{\gamma_y}{\gamma} \Phi_y(P_i, \tilde{q}_j) + \frac{\gamma_z}{\gamma} \Phi_z(P_i, \tilde{q}_j) + \frac{1}{\gamma} \frac{\partial \gamma}{\partial H} \Phi(P_i, \tilde{q}_j) \tag{38}$$

and

$$\begin{aligned} g_{tij} = \frac{\gamma_x}{\gamma} \tilde{\mu}_j \frac{\partial \Phi_x(P_i, q)}{\partial q_t}\bigg|_{q=\tilde{q}_j} + \frac{\gamma_y}{\gamma} \tilde{\mu}_j \frac{\partial \Phi_y(P_i, q)}{\partial q_t}\bigg|_{q=\tilde{q}_j} \\ + \frac{\gamma_z}{\gamma} \tilde{\mu}_j \frac{\partial \Phi_z(P_i, q)}{\partial q_t}\bigg|_{q=\tilde{q}_j} + \frac{1}{\gamma} \frac{\partial \gamma}{\partial H} \tilde{\mu}_j \Phi_t(P_i, \tilde{q}_j) \qquad , \qquad t \,\epsilon\, \{x, y, z\} \end{aligned} \tag{39}$$

The system that needs to be solved becomes:

$$\begin{bmatrix} \Delta a_1 \\ \Delta a_2 \\ \vdots \\ \Delta a_m \end{bmatrix} = \begin{bmatrix} \boldsymbol{h}_{11} & \boldsymbol{h}_{12} & \cdots & \boldsymbol{h}_{1n} \\ \boldsymbol{h}_{21} & \boldsymbol{h}_{22} & \cdots & \boldsymbol{h}_{2n} \\ \vdots & \vdots & \ddots & \vdots \\ \boldsymbol{h}_{m1} & \boldsymbol{h}_{m2} & \cdots & \boldsymbol{h}_{mn} \end{bmatrix} \begin{bmatrix} \boldsymbol{x}_1 \\ \boldsymbol{x}_2 \\ \vdots \\ \boldsymbol{x}_n \end{bmatrix} \tag{40}$$

where:

$$\Delta a_i = a_i - \tilde{a}_i \quad , \quad \boldsymbol{h}_{ij} = (g_{ij} \;\; g_{xij} \;\; g_{yij} \;\; g_{zij}) \;\; \text{and} \;\; \boldsymbol{x}_j = (\Delta\mu_j \;\; \Delta q_{xj} \;\; \Delta q_{yj} \;\; \Delta q_{zj})^T \tag{41}$$

Equation (40) can only be solved if the number of measurements is larger than or equal to four times the number of point masses ($m \geq 4n$). This means that in regions with few gravity measurements, it is not possible to reliably compute a large number of point masses. Clearly, the free-positioned point-mass technique is less robust than the fixed-positioned point-mass technique, and as such, is sensitive to the gravity data used.

The elements of the design matrix can be computed in geocentric Cartesian coordinates {x, y, z} by inserting the base vectors from equation (4):

$$\Phi_s(P_i, \tilde{q}_j) = \frac{(\tilde{q}_{sj} - P_{si})}{l^3(P_i, \tilde{q}_j)} \qquad , \qquad s \,\epsilon\, \{x, y, z\} \tag{42}$$

and

$$\left.\frac{\partial \Phi_s(P_i,q)}{\partial q_t}\right|_{q=\tilde{q}_j} = \frac{\delta_{st}}{l^3(P_i,\tilde{q}_j)} - 3\frac{\tilde{q}_{tj}-P_{ti}}{l^5(P_i,\tilde{q}_j)}(\tilde{q}_{sj}-P_{si}) \qquad , \qquad s,t\,\epsilon\,\{x,y,z\} \tag{43}$$

where δ_{st} is the well-known Kronecker-delta:

$$\delta_{st} = \begin{cases} 1 & \text{for} \quad s = t \\ 0 & \text{for} \quad s \neq t \end{cases} \tag{44}$$

The (unweighted) least-squares estimates of the vectors $\boldsymbol{x}_j$ in equation (41) can now be computed with equation (36). This will give corrections to the approximate values for the magnitudes and positions of the point masses. This leads to new approximations which then can be used again as input and new corrections can be calculated. This process can be repeated iteratively until the corrections are smaller than some predetermined value or until a predetermined number of iterations is reached. The latter method was used in this study.

Any numerical stability problems in computing the corrections cannot be excluded, especially when the point masses are close together, which decreases the orthogonality of the base vectors (Barthelmes, 1986). The least-squares solution can be modified in order to account for these stability problems using a regularisation method. With the regularisation method of Tikhonov (eg. Kuhnert, 1976) the solution of equation (36) becomes:

$$\hat{\boldsymbol{x}} = (A^T A + \boldsymbol{\alpha} I)^{-1} A^T \boldsymbol{y} \tag{45}$$

where $\boldsymbol{\alpha}$ is the vector containing real-numbered regularisation parameters and I is the identity matrix.

Summary of the algorithm

The n-th step of the algorithm by Barthelmes (1986) can now be formulated verbally as follows (Barthelmes & Dietrich, 1991):

1. Subtraction of the gravity anomalies produced by the $(n-1)$ point masses from the measurements to give residuals (equation 23).
2. Selection of the position P_{max} of the maximum absolute value of the residuals (equation 21).
3. a) Determination of the approximate value for the n-th point mass position by placing it directly below the point P_{max} at a starting depth D_0 (equation 25).
   b) Determination of the magnitude of the new point mass (equation 35).
   c) Iterative improvement of the magnitude and position of the new point mass by non-linear optimisation (equation 40).

4. Selection of those point masses among the $n-1$ previous masses up to a fixed number N_ε which have the smallest distance up to the n-th point mass.
5. Iterative improvement of magnitudes and positions of the n-th point mass together with the selected neighbouring masses by non-linear optimisation (equation 40).

THE DATA USED FOR THE EXPERIMENTS IN WESTERN AUSTRALIA

Part of the 1992 data release of the Australian Geological Survey Organisation's (AGSO) national gravity database was used for the point-mass modelling experiments in the Perth region. The more recent data releases were not used because, firstly, the 1992 data release has been subjected to a number of data cleaning processes and gravity anomalies recomputed using stricter geodetic approaches (eg. Featherstone *et al.*, 1997), and secondly, no new data have been added to the AGSO database in this region during subsequent updates. The datum for the AGSO gravity measurements is IsoGal84 (Wellman et al. 1985). The subset used contains a total of 6,284 land and shipboard gravity observations over the region bound by $-33.50^\circ \leq \phi \leq -30.75^\circ$ and $115^\circ \leq \lambda \leq 117^\circ$ (Figure 2).

Figure 2 shows a generally denser spatial coverage of AGSO's gravity observations on land to the west of the Darling Fault (situated approximately along the 116° meridian). The coverage in this area has been improved for geophysical studies of the geological structure of the Perth Basin (eg. Dentith *et al.*, 1993). The observations generally follow roads and tracks along which spirit-levelled AHD benchmarks exist, whereas the relatively sparse observations to the east of the Darling Fault have had their heights determined using barometric methods (eg. Fraser *et al.*, 1976). The AHD benchmark heights are considerably more accurate, say $\sim$5cm, than the barometric heights, say $\sim$4-6m. This reduces the error in the gravity anomalies computed on land to the west of the Darling Fault. Accordingly, there is a disparity in the spatial coverage and accuracy of the land gravity anomalies on either side of the Darling Fault.

There is another disparity in the gravity data coverage and quality in the study area. A combination of limited marine vessel accessibility and instability due to wave-action currently make it impossible to collect sufficiently accurate marine gravity observations very close to the coast. The close proximity of the study area to the Indian Ocean dictates that marine gravity observations cannot be made to satisfy the requirement of homogeneous gravity data coverage. It can be seen in Figure 2 that the AGSO shipboard gravity observations are very sparse and most ship-track measurements are to the west of Rottnest Island (115.5°, -32°). This is where airborne gravimetry can make a major contribution to gravity field determination and modelling, though no such data are yet available in this region.

In this and previous studies (eg. Johnston and Featherstone, 1998), an attempt was made to supplement the AGSO shipboard gravity observations by satellite altimeter-derived gravity anomalies

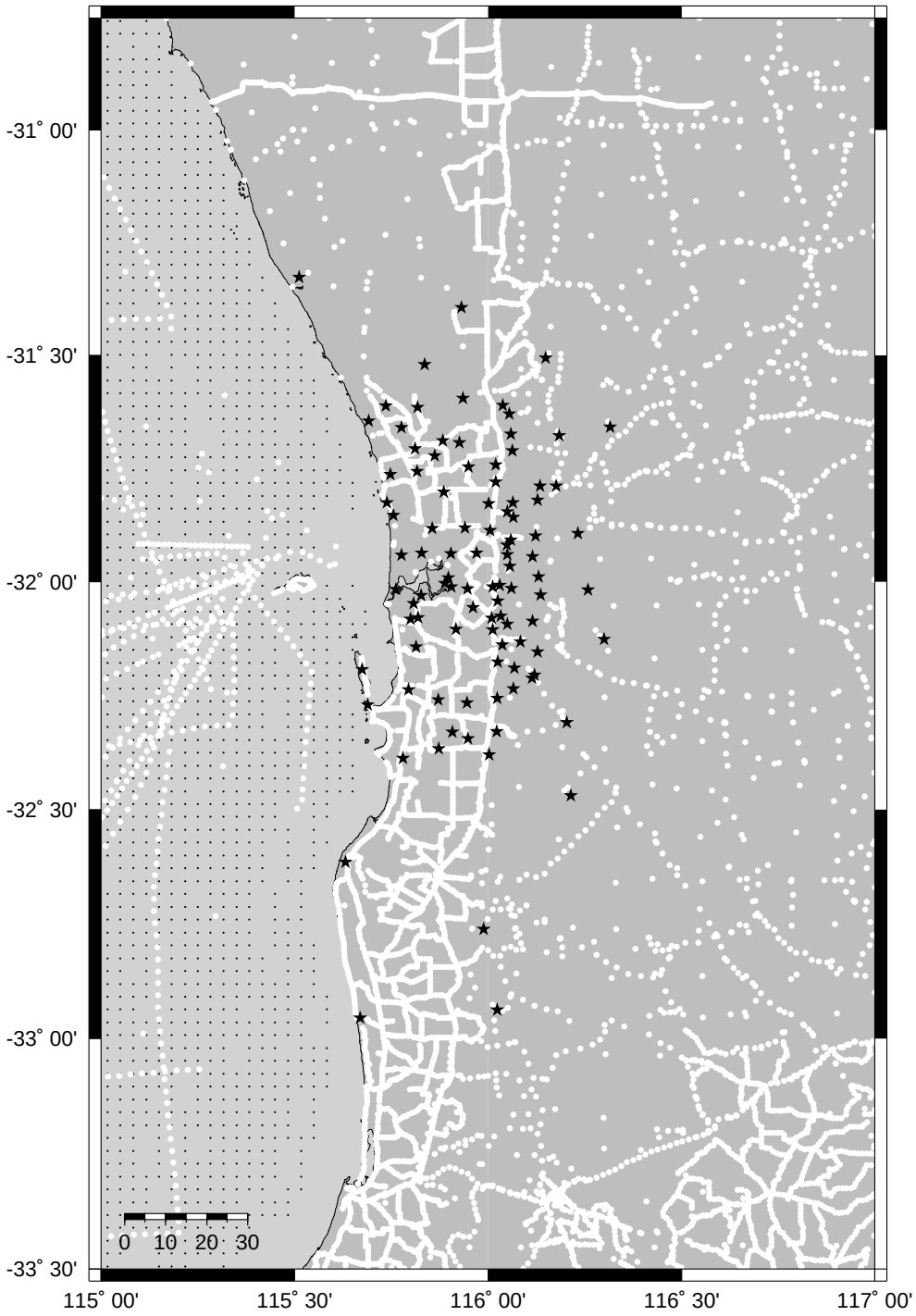

Fig. 2. Spatial distribution of the AGSO land and shipboard gravity data (white circles), the satellite altimeter data (black dots) and GPS-levelling data (black stars)

(Figure 2). The 1369 gravity anomalies (assumed to be free-air) used in this study have been computed on a 2' by 2' grid from a combination of Geosat, TOPEX/Poseidon and ERS-1 satellite altimeter missions by Sandwell and Smith (1997). However, satellite altimeter data are known to be erroneous close to the coast (demonstrated later). This is because they are affected by loss of signal lock through back scattering from the land (eg. to the north-east of Rottnest Island in Figure 2), un-modelled near-shore sea-surface topography (eg. due to the outflow of fresh water from the Swan River) and poorly modelled shallow-sea tides. In AUSGeoid98 (eg. Johnston and Featherstone, 1998; Featherstone *et al.*, 2001), the AGSO and satellite-altimeter gravity data were combined using least-squares collocation (Kirby and Forsberg, 1998). However, only the discrete gravity measurements will be used in this study, which avoids the errors introduced by the gridding processes, but does not allow for such merging of the AGSO and satellite altimeter data.

Due to the quality, mixed measurement types and spatial coverage of the gravity data in the study area (Figure 2), it does not present an ideal 'field laboratory', though it does provide a challenging one. Moreover, the gravity data coverage and accuracy are not the only reasons for the relatively poor performance of previous attempts at gravimetric geoid modelling in the Perth region. The large topographic mass-density contrast across the Darling Fault, which reaches over 500kgm^{-3} in some places, causes a large perturbation of the Earth's gravity field. For example, there is a horizontal gradient of the free-air gravity anomaly of $\sim$100mGal over $\sim$15km (Figure 5).

Geodetic GPS networks that are co-located with orthometric heights provide discrete, geometrical control on gravimetric geoid modelling on land. Strictly speaking, however, this yields the separation between the local vertical datum and the reference ellipsoid and is therefore subject to several errors (eg. Featherstone 1998). The 99 GPS data used for this study (Figure 2) come from a geodetic network observed by the Western Australian Department of Land Administration for the study by Featherstone (2000). This GPS network is tied to the ITRF92 (epoch 94.0) reference frame as part of the implementation of the Geocentric Datum of Australia. The error estimate of these GPS-derived ellipsoidal heights is $\sim \pm$12mm (Featherstone, 2000), but this is in relation to the STATEFIX network (Stewart *et al.*, 1997) and a larger uncertainty, say $\sim$10cm, exists in relation to the ITRF92 (epoch 94.0).

The accuracy of the 99 co-located third-order spirit-levelled heights and definition and realisation of the AHD are more problematic. For instance, the AHD uses a normal orthometric height system. Helmert orthometric corrections based on observed gravity data reach $\sim$-4.8mm over $\sim$14km across part of the Darling Fault, whereas the normal orthometric corrections are $\sim$0.1mm over the same east-west traverse (Allister and Featherstone, this issue). The Perth region also presents an exception from the AHD (strictly speaking, a separate vertical datum) because the heights based on the Fremantle tide gauge were retained in preference to the adjustment of the AHD. Instead, a buffer zone

was introduced between the Fremantle-based heights and the adjusted AHD heights (Roelse *et al.* 1971).

METHODS AND RESULTS

In order to apply the free-positioned point-mass modelling technique to a local area, it is first important to note that local gravity data alone can never properly determine the low frequencies of the Earth's gravity field spectrum. Therefore, in this investigation, use is made of the so-called remove-compute-restore technique (eg. Vermeer, 1998; Ihde *et al.*, 1998; Denker *et al.*, 1999). This means that the gravity anomalies according to spherical harmonic degrees 2 to 360 of the EGM96 global geopotential model (Lemoine *et al.*, 1998) were first subtracted from the gravity anomalies computed from the measurements. After the point mass computations, the geoidal influence of these low frequencies was restored.

The residual geoid heights generated by the point masses (N_{PM}) were computed using Bruns's equation (6), where the disturbing potential was computed with equation (5). This gives

$$N_{PM}(P) = \frac{G}{\gamma} \sum_{i=1}^{n} \frac{m_i}{l(P, q_i)} \tag{46}$$

where all terms have been defined earlier. The geoid heights were computed at the positions of the 99 GPS-levelling points (Figure 2), so that a direct comparison with the GPS-levelling heights was possible. Importantly, the positions and magnitudes of the point masses were computed from observed gravity data taken from a large area around the GPS-levelling points ($-33.50° \leq \phi \leq -30.75°$ and $115° \leq \lambda \leq 117°$). This was found necessary to avoid inconsistencies at the edges (i.e. edge effects of limited data coverage).

Parameters to be optimised

Barthelmes's free-positioned point-mass software was used for the computation of magnitudes and positions of the point masses (Barthelmes, 1986). In this software, a number of parameters need to be defined prior to the computation. The main parameters that were varied during the investigation to get the best fit to the GPS-levelling data are:

1. Total number of point masses: The addition of each new point mass decreases the root mean square of the differences between the observed and computed gravity anomalies, but also decreases the redundancy.
2. Depth limits of the point masses: The point masses need not be too deep, because the low frequencies are already given by the EGM96 global geopotential model. More importantly, the deeper the point masses are, the less orthogonal the base vectors become (described earlier). The

point masses should not be too shallow because the gravity data distribution is limited (Figure 2).

3. Direction of optimisation: The position of each new point mass can be optimised in all directions (tangential and radial) or in radial direction only. When the point masses are allowed to be optimised in all directions, they tend to be positioned in gaps in the coverage of the gravity data. This effect was avoided using radial optimisation only.
4. Number of iterations for each new point mass: The magnitude and position of each new point mass needs to be optimised by iteration. The number of iterations in the radial and tangential directions can be different. After the optimisation of the new point mass alone, the new point mass and its neighbouring point masses are then optimised together. The number of iterations in this optimisation can also be given separately for the radial and tangential directions. This gives a total of four iteration parameters that can be varied.
5. Number of neighbouring point masses: Ideally, for each new point mass the position and the magnitude of this and all other point masses need to be recomputed. However, this is a very time consuming process. Barthelmes (1986) has shown that it is sufficient to optimise only a certain number of neighbouring point masses when the base vectors of the point masses are nearly orthogonal. The number of recomputed neighbouring point masses was increased when the base vectors were not sufficiently orthogonal.
6. Regularisation parameters: The regularisation parameter α in equation (45) can be specified separately for the radial and tangential optimisations. To control the regularisation, the parameter α is multiplied by a certain parameter (increase factor) when the root mean square of the fit to the gravity anomalies is increasing, or divided by another parameter (decrease divisor) when the root mean square is decreasing. This gives a total of four regularisation variables.

It is very difficult to simultaneously determine the optimal values for all the above parameters that lead to a point-mass geoid model which fits the GPS-levelling data the best. Instead, a few combinations of these parameters were investigated based on earlier experiences of the third author in other test areas.

Number of point masses

The left-hand-side of Figure 3 shows a contour map of the geoid heights derived from EGM96 and 500 free-positioned point masses, based on land, shipboard and altimeter data. Table 1 shows the parameters that were used to obtain this result. The black filled circles in Figure 3 show the positions of positive mass disturbances and the unfilled circles show the positions of negative mass disturbances. The right-hand-side of Figure 3 shows a map of the differences between the point-mass geoid heights and the GPS-levelling heights.

1	total number of point masses	500			
2	depth limits (upper and lower)[meters]	1000	80000		
3	direction of optimisation	all			
4	number of iterations for each new point mass (radial, tangential, radial+neighbours, tangential+neighbours)	7	7	20	10
5	number of neighbouring point masses	10			
6	regularisation parameters (radial, tangential, increase factor, decrease divisor)	10^{-12}	10^{-12}	200	50

Table 1. The parameters used to generate the point-mass geoid model in Figure 3

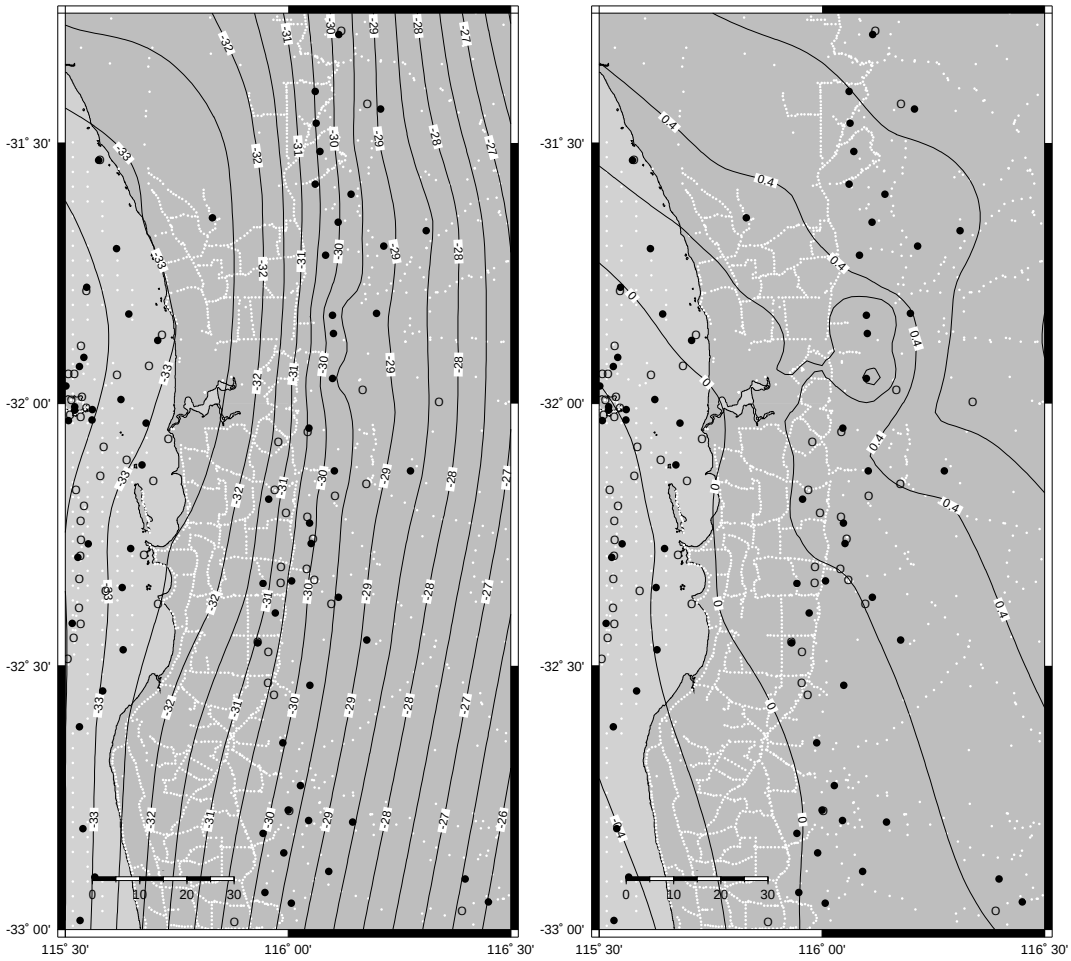

Fig. 3. left: the point-mass geoid model computed from the parameters specified in Table 1; right: the differences between the point-mass geoid and the 99 GPS-levelling data (cf. Figure 2) (black circles: positive point masses; clear circles: negative point masses; contours in meters at an interval of 0.5m (left) and 0.2m (right)).

Using 500 point masses, the redundancy is still high for the complete study area. For every free-positioned point-mass, four unknowns need to be computed (three for the position and one for the magnitude). This means that a total number of 2,000 unknowns were computed from 7,653 gravity data, which gives a high redundancy of 5,653. By definition, the root mean square of the differences between the observed gravity anomalies and the gravity anomalies generated by the point masses decreases as each new point mass is added. It was, however, found that the differences between the point-mass generated geoid heights and the GPS-levelling heights did not decrease in the Perth area after increasing the number of point masses beyond 500 (Table 2). Therefore, the solution with 500 point masses is the best of the solutions tested, but this statement is subject to the errors in the GPS-levelling data (described earlier).

number of point masses	root mean square of the fit to the gravity anomalies (mGal)	standard deviation of the fit to the geoid to GPS-levelling (cm)
EGM96 only	-	26.5
10	20.85	35.3
50	8.98	23.3
200	3.37	18.2
500	1.84	17.5
1000	1.37	19.0

Table 2. The fit of gravity anomalies and geoid heights for different numbers of point masses (the other parameters and data used to create these figures will be discussed later).

The best fit to the GPS-levelling data is found with the use of 500 point masses. The standard deviation of 17.5cm is slightly larger then the fits of other geoid models (Table 3). It is important to note that the error budget of the GPS-data is $\sim$12mm and, say, $\sim$50mm for the AHD. Therefore, the differences in Tables 2 and 3 are not significant when errors in the GPS-levelling data are considered.

geoid model	standard deviation (cm)
best point-mass model	17.5
AUSGeoid93 (Steed and Holtznagel, 1994)	13.6
EGM96 only (Lemoine *et al.*, 1998)	26.5
AUSGeoid98 (Featherstone *et al.*, 2001)	13.0
Combined AUSGeoid98 (Featherstone, 2000)	1.0*

Table 3. Standard deviation of the fit of several geoid models to 99 GPS-levelling data in the Perth region.
* This small value results from a least-squares collocation fit

Using point masses to identify density contrasts

In Figure 3, a large number of point masses are situated along the Darling Fault (approx. $116°$E), as could have been expected. The Darling Fault produces a large horizontal gradient in the gravity data (Figure 5), which can only be modelled with high frequency information. The closely spaced point masses provide this high frequency data. There is a clear trend in the differences between the geoid and GPS-levelling (Figure 3 right) from small differences near the coastline to higher differences in the hills. There is also a clear depression in the differences at ($-31.9°$, $116.2°$) with three large, shallow, positive point masses.

These point masses are "lifting up" the geoid (and therefore "pulling down" the differences). This feature can also be seen in the curvature of the contour lines near these point masses in the left map of Figure 3. These point masses have been positioned in areas where there is no gravity data coverage (Figure 3), because radial and tangential optimisation was chosen for this particular point-mass modelling (Table 1). Since these point masses must generate gravity consistent with the observations surrounding the data gaps, the magnitudes of the point masses become large,and their depths shallow. Therefore, when these same masses are used to compute the geoid (equation 46), very large geoid values occur directly above the masses. Therefore, as with all geoid modelling techniques, the complete coverage of the gravity data is a critical issue.

An obvious solution for preventing the point masses from being positioned in the gravity data data gaps is to optimise their positions in a radial direction only. This used 10 iterations for the new point mass only and 20 iterations with its neighbours. However, without the tangential optimisation, the numerical instabilities in the matrix inversion became larger. Therefore, the radial regularisation parameter was chosen as $\alpha = 10^{-3}$ instead of $\alpha = 10^{-12}$ and the increase factor was also raised from 200 to 400 (cf. Table 1). Furthermore, the number of neighbouring point masses that were computed was raised from 10 to 20. This computation, and computations with several other choices for the parameters, showed that the numerical instabilities when using gravity data in this study area were too large for the regularisation to be effective.

Using point masses to identify shipboard gravity data errors

The reason for these instabilities can be seen in Figure 4, which shows the positions of 200 point masses computed with the aforementioned parameters. These point masses are clustering along the ship tracks, especially along one ship track north-west of Rottnest Island. The reason for this is that the altimeter data and the AGSO shipboard gravity data are not consistent. Therefore, a lot of point masses are needed to compensate for the jump in gravity anomaly values. The inconsistency between the two data sets can best be seen from a profile of the gravity data between the latitudes $31.85°$ and $31.95°$ (Figure 5). This is the shaded band in Figure 4.

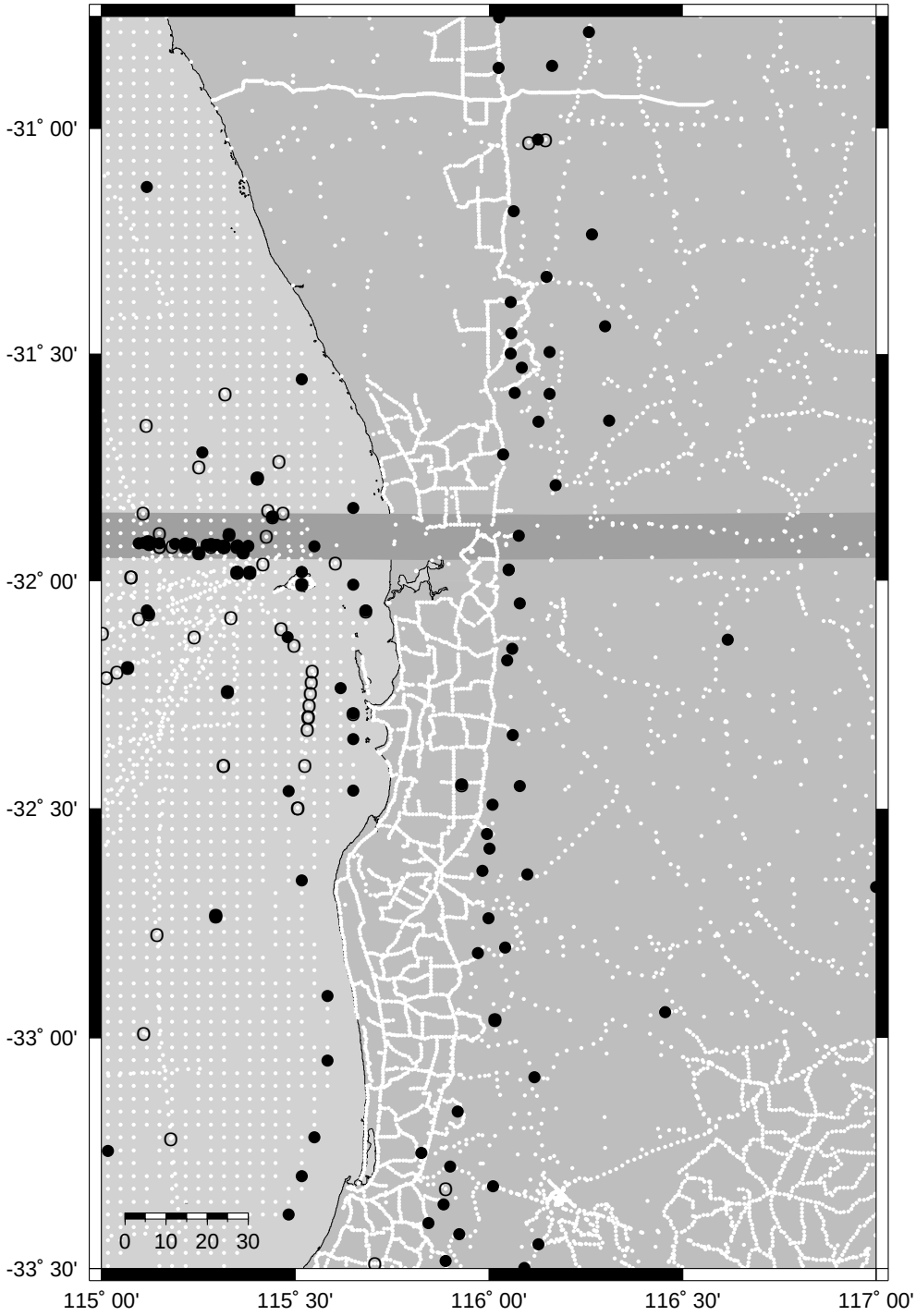

Fig. 4. The positions of 500 point masses (black positive; clear negative) in relation to land, shipboard and altimeter gravity data (white circles). The distinction among the different gravity data is made in Figure 2. The shaded band shows the area that was used to generate the profile in Figure 5.

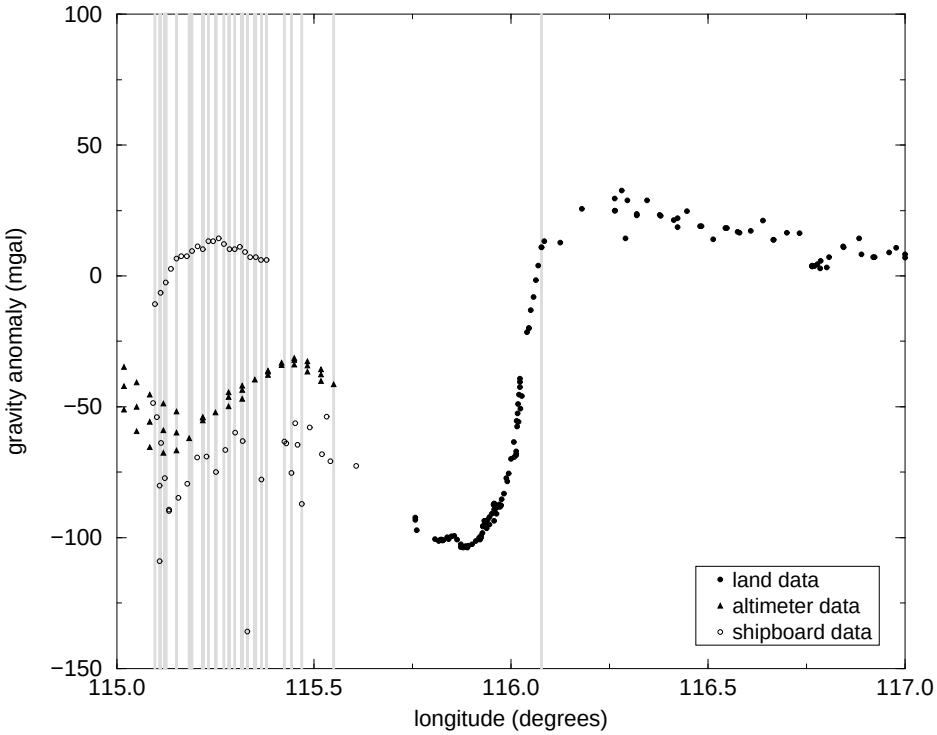

Fig. 5. Free-air gravity anomaly profile of land, altimeter and shipboard data over latitudes between 31.85° and 31.95° (see shaded band in Figure 4). The vertical lines show the positions of the point masses (see circles in Figure 3.

In Figure 5, the shipboard data are very scattered with differences up to ∼150mGal over distances less than 10km. These differences are very unlikely to be caused by geological features; the quality of the shipboard data is obviously very bad. The AGSO shipboard data have not been cross-over adjusted, which is clear from the bias in the track shown in Figures 4 and 5. As the shipboard data are not stored in a format that can be cross-over adjusted, they were simply removed (429 points). Another point-mass geoid model was then computed using the parameters in Table 4. Here, the upper depth limit was increased (cf. Tables 1 and 4) to try to prevent the masses from being positioned in the gravity data gaps, while also overcoming the numerical stability problems described earlier. These choices of parameters resulted in the geoid computation with the least numerical instabilities of all (described next).

1	number of point masses	500			
2	depth limits (upper and lower limit)	3000	50000		
3	direction of optimisation	all			
4	number of iterations (radial, tangential, radial+neighbours, tangential+neighbours)	7	7	20	10
5	number of neighbouring point masses	20			
6	regularisation parameters (radial, tangential, increase factor, decrease divisor)	10^{-3}	10^{-12}	200	50

Table 4. The parameters used to generate the point-mass geoid model in Figure 6

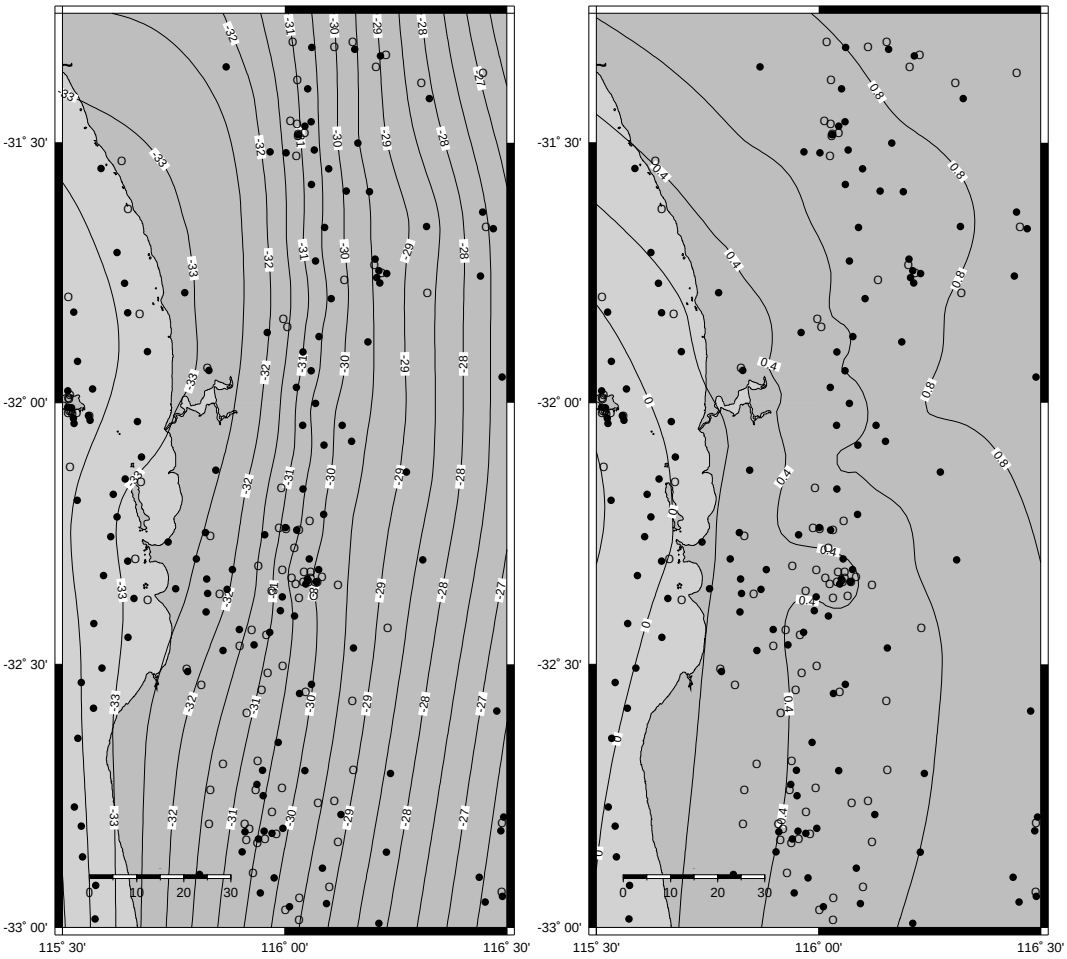

Fig. 6. left: the geoid computed from 500 point masses; right: the differences between the geoid and the GPS-levelling data (black circles: positive point masses; clear circles: negative point masses; contours in meters at an interval of 0.5m (left) and 0.2m (right)).

Orthogonality testing

The results in Figure 6 show that many more point masses are situated on the land areas. This time, however, there are a lot of point masses near Rottnest Island, but the masses along the ship tracks have disappeared (cf. Figure 3), as was to be expected. A problem is that a lot of point masses very close to each other cause numerical instabilities in the point mass computation. When the point masses are too close together, the orthogonality of the base vectors in equation (4) decreases. It is very important that these base vectors are nearly orthogonal, otherwise the iterative nature of the method, where only a number of point masses are recomputed in each step, becomes invalid. The orthogonality of the base vectors of the point masses, i.e. the angles α_{ij} in Hilbert space between the base vectors of the point masses, can be computed by (Barthelmes, 1986):

$$\alpha_{ij} = \arccos\left((1-R_i^2)(1-R_j^2)(1-R_iR_j\cos\Psi_{ij})(1+(R_iR_j)^2-2R_iR_j\cos\Psi_{ij})^{-\frac{3}{2}}\right) \tag{47}$$

where Ψ_{ij} is the spherical distance between the two point-mass positions and R_i and R_j are the quotients of the distance between the point mass and the geocentre and the Earth's radius. In the cases of 500 and 1000 point masses, more than 80% of all the possible combinations of computed point masses have an angle in the Hilbert space that is greater than 89°, which shows that most of the base vectors are nearly orthogonal. Figure 7 shows that the percentage of angles below 50° is approximately equal for 200 and 500 point masses, but gets higher in the case of 1000 point masses. This might be an explanation for the worse fit to the GPS-levelling data in the case of 1000 point masses (Table 2).

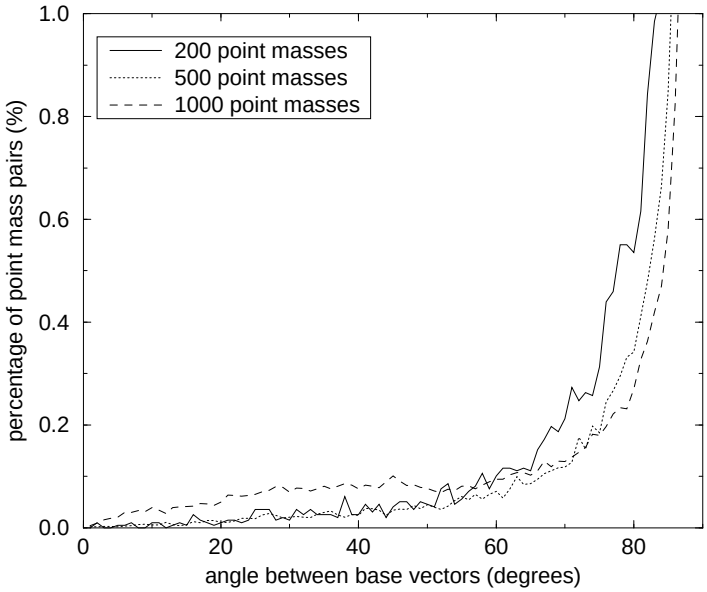

Fig. 7. Percentage of angles in the Hilbert space between base vectors for 200, 500 and 1000 point masses

The trend in the differences between the point-mass derived geoid and the GPS-levelling data (Figure 6 right) is however still the same: small differences near the coastline and large differences in the east. Several tests with other regularisation parameters and other numbers of point masses did not yield any better results. Although the shipboard data was removed, the instabilities still became too large when the point masses were only optimised in the radial direction, even when the number of iterations for the new point mass with its neighbours was increased to 30 and the increase factor in the regularisation was raised to 600. This radial-optimisation-only-mode has, however, proven to be very useful in tests by the third author in areas with a less problematic data set.

The point-mass derived geoid could be improved significantly by applying a bias and tilt or using least-squares collocation to model the residuals (Featherstone, 2000). However, this obscures the problems central to point-mass modelling and our original aim of determining errors in the Australian Height Datum.

Using point masses to identify land gravity data errors

After the removal of the shipboard gravity data, several clusters of point masses appear in Figure 8. These are grouped along the Darling Fault, on Rottnest Island and at $-33.4°$, $116.25°$. In order to determine the cause of these clusters, four profiles are plotted for various latitudes in Figure 9. All the profiles have a width of 0.1° and are situated respectively around 30.80°, 32.00°, 32.35° and 33.35° (Figures 8 and 9).

From Figure 9 it can be clearly seen that all the point masses are positioned in places where there is a discontinuity in the gravity anomalies. The point masses provide the high-frequency information that is needed to model these discontinuities, which can either indicate a geological feature or an error in the gravity data. Although the Perth region contains a large mass-density difference over the Darling Fault, most point masses appear to cluster in areas with errors in the gravity data.

The sensitivity of point-mass modelling to inconsistencies in the gravity data causes the method not to perform well in areas with poor gravity data quality or poor spatial data coverage. However, this makes the point-mass method an excellent way to find inconsistencies or errors in the data. For instance, the large number of point masses under Rottnest Island can easily be understood by looking at Figure 9b. The AGSO land gravity data on the island (at $115.5°$E) differ from the altimeter data around the island up to about 40mGal over a very small distance.

It is a well-known fact that the quality of altimeter data gets poor near the coastline (described earlier). There is a large difference between the altimeter data and the land data in the profiles in Figure 9 (except for Figure 9a). To achieve a geoid computation in the Perth region with centimeter accuracy will only be possible if either shipboard, altimeter or airborne gravity data with better quality becomes available in the coastal areas. Alternatively, techniques to improve satellite altimeter data in the coast must be developed.

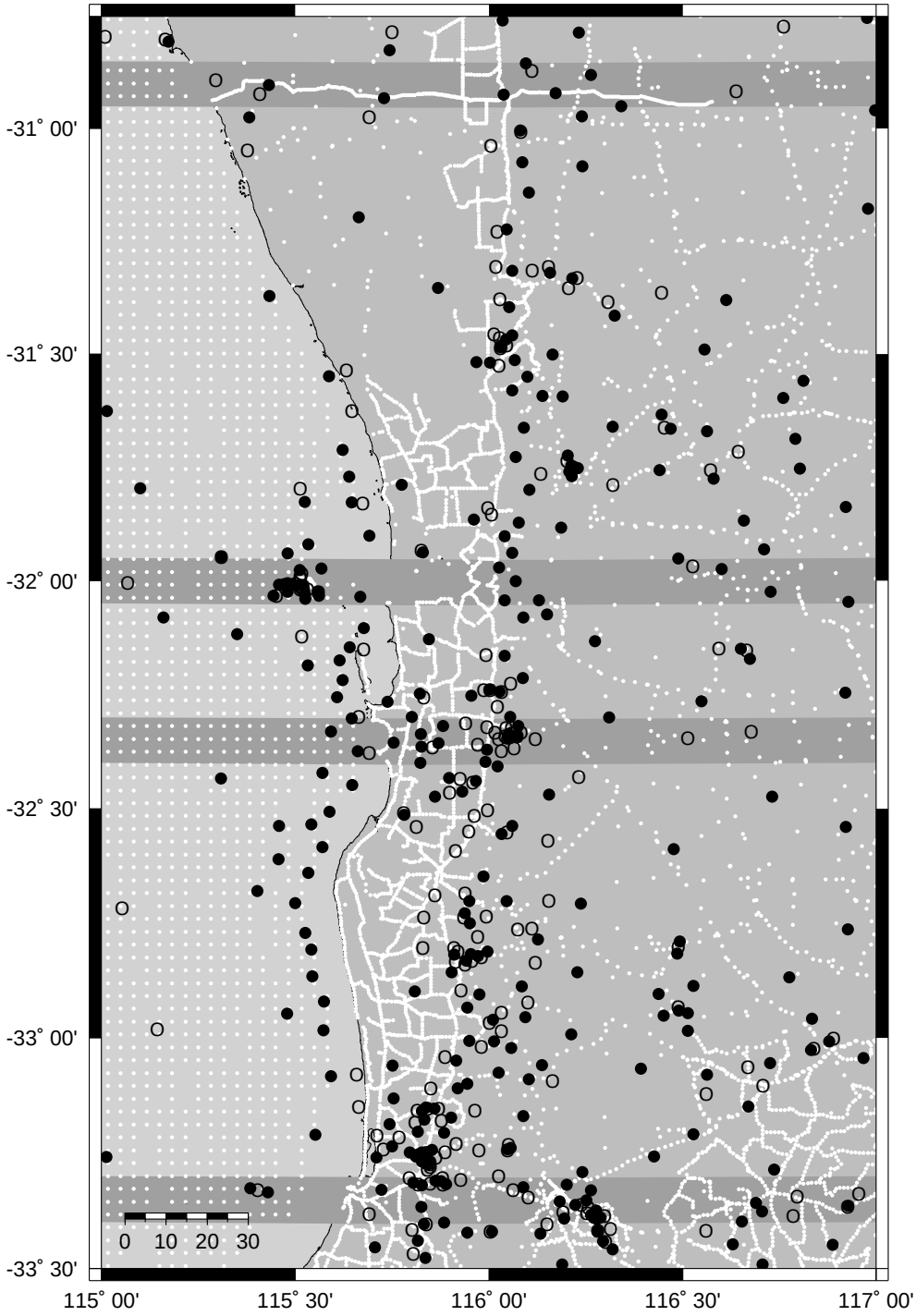

Fig. 8. The positions of 500 point masses (black positive; clear negative) determined from AGSO land data and satellite altimeter data only (white circles). The distinction among the different gravity data is made in Figure 2. The shaded bands show the areas that were used to generate the profiles in Figure 9.

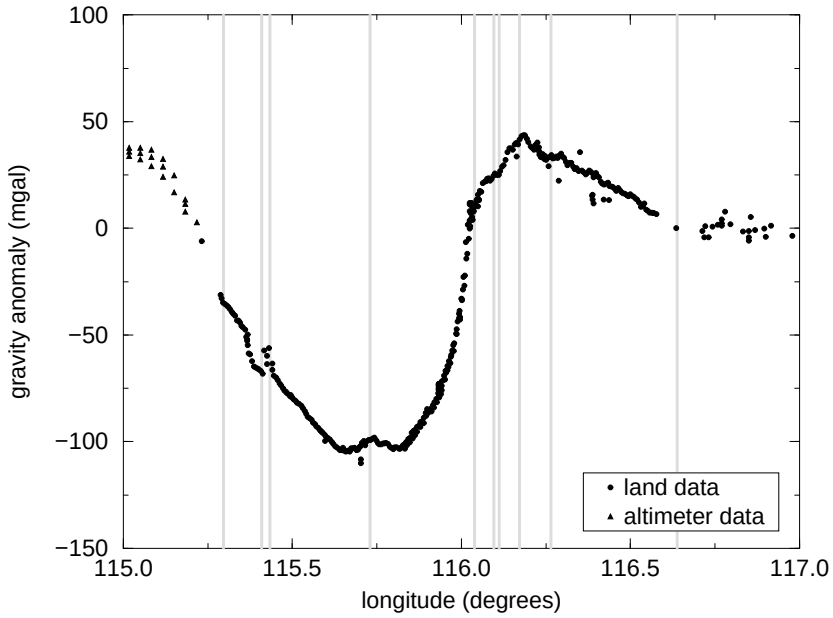

(a)

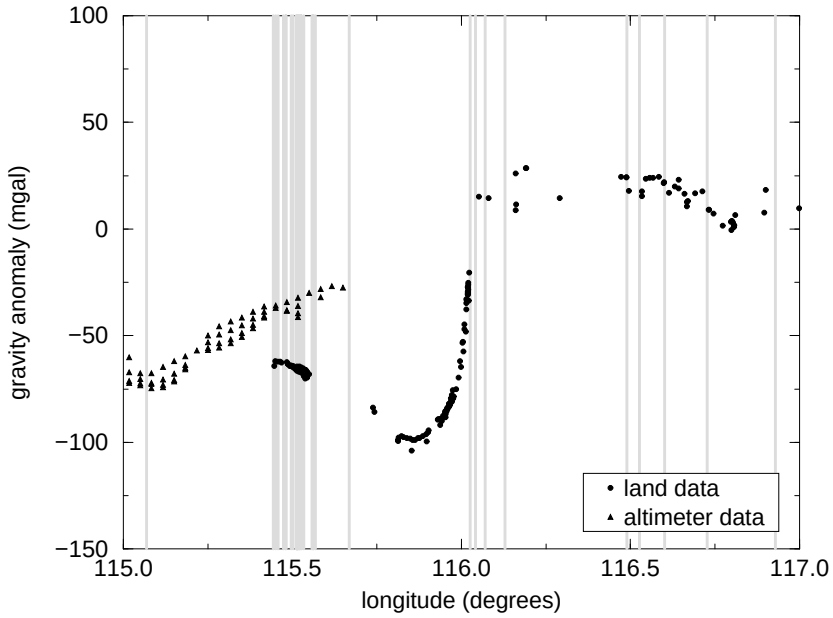

(b)

Fig. 9. Free-air gravity anomaly profile over latitudes between: (a) 30.85° and 30.95°; (b) 31.95° and 32.05°. The vertical lines show the positions of the point masses (see circles in Figure 8)

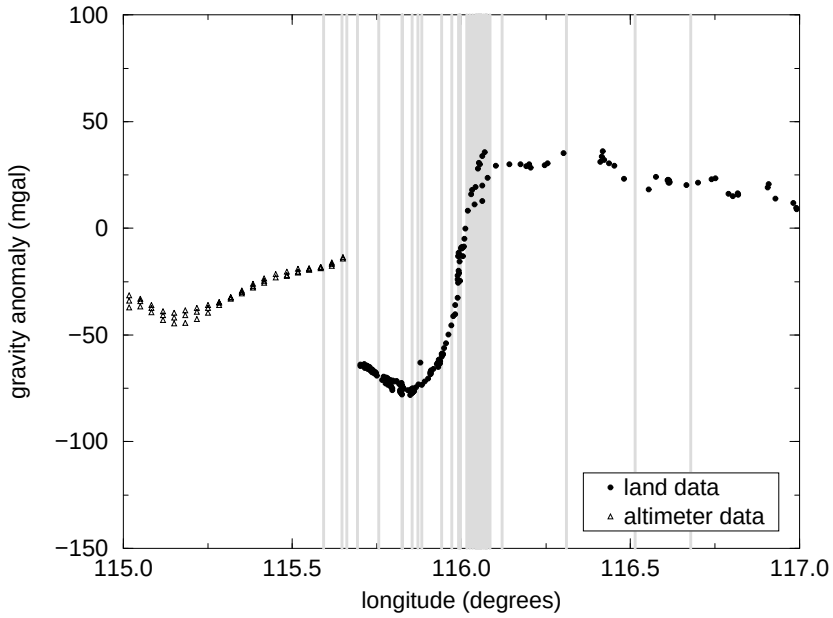

(c)

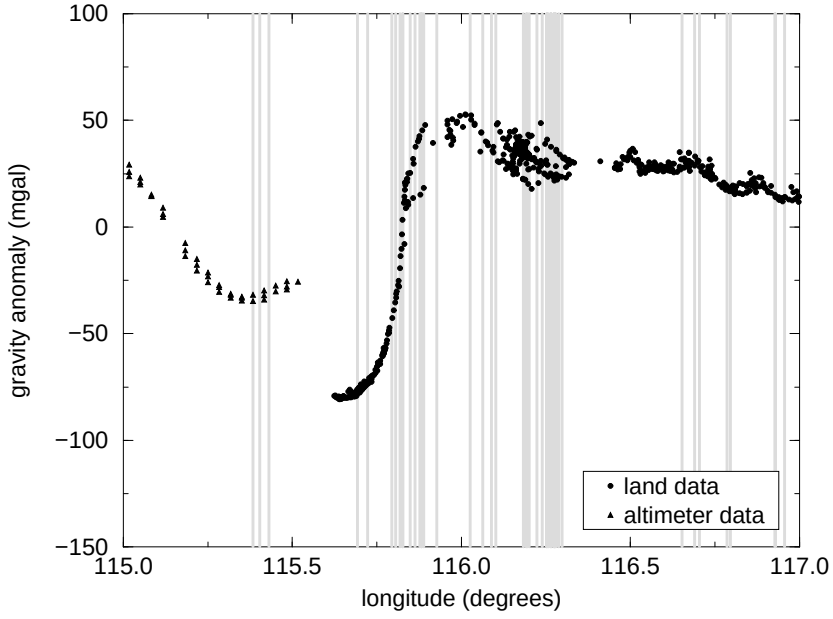

(d)

Fig. 9. gravity anomaly profile + positions of point masses over latitudes between: (c) 32.30° and 32.40°; (d) 33.30° and 33.40°. The vertical lines show the positions of the point masses (see circles in Figure 8)

CONCLUSIONS

Any inconsistencies in the Australian Height Datum in the Perth region could not be detected with the use of a free-positioned point-mass gravity field modelling technique. The main difficulty is that this point-mass algorithm is very sensitive to the inconsistent gravity data types and coverage in the area. This causes the point masses to cluster in the neighbourhood of this inconsistent data, and when these point masses are close together, numerical stability problems occur. Applying different weights to the different data qualities in the least-squares inversion might deliver some improvements, but this was not tested in this study. However, the profiles of the data clearly show that there are systematic differences between the data, which would have to be modelled irrespective of a least-squares weighting strategy.

The data gaps in the study area also adversely influenced the results. Many point masses tended to position in the gravity data gaps. The apparent solution to prevent the point masses from moving tangentially (by optimising them in a radial direction only), did not improve the results to any great extent. Moreover, the numerical instabilities became larger, causing errors in the inversion of the matrix in the least-squares optimisation. Although the free-positioned point-mass method does not make a significant improvement in the fit to GPS-levelling data over methods based on Stokes's integral, it has a complementary application as follows.

The sensitivity of the free-positioned point-mass method to inconsistencies in the data makes this very useful for detecting these inconsistencies. A cluster of point masses can point out a striking geological feature (eg. the Darling Fault), but appears in many other cases to be caused by data inconsistencies. The poor quality of the various gravity data types in the Perth region has been shown, especially over the ocean. Therefore, data of a better quality is needed to compute a geoid that is sufficiently precise to give information on the quality of the Australian Height Datum.

Finally, despite the poor performance of the point-mass technique in the challenging Perth region, it should not be discounted from use in future Australian geoid modelling.

ACKNOWLEDGEMENTS

We would like to thank the following organisations for their supply of data: Australian Geological Survey Organisation, Western Australian Department of Land Administration, US National Aeronautical and Space Administration, US National Imagery and Mapping Agency, and Scripps Institute for Oceanography. This research was supported financially by a travel grant from Delft University of Technology to Claessens and an ARC large grant A00001127 to Featherstone.

REFERENCES

Allister, N. and W.E. Featherstone (this issue) Determination of Helmert orthometric heights using digital barcode levelling, observed gravity and topographic mass-density data over part of the Darling Scarp, Western Australia. *Geomatics Research Australasia*.

Barthelmes, F. and H. Kautzleben (1983) A new method of modelling the gravity field of the Earth by point masses. Proceedings of the XVIII General Assembly of the IUGG, Hamburg, August, 442-447.

Barthelmes, F. (1986) Untersuchungen zur Approximation des äußeren Schwerefeldes der Erde durch Punktmassen mit optimierten Positionen. Report Nr. 92, Veröffentlichungen des Zentralinstitut Physik der Erde, Potsdam.

Barthelmes, F. (1989) Local gravity field approximation by point masses with optimized positions. Report Nr. 102(2), Veröffentlichungen des Zentralinstitut Physik der Erde, Potsdam.

Barthelmes, F. and R. Dietrich (1991) Use of point masses on optimized positions for the approximation of the gravity field. In: *Determination of the Geoid: Present and Future*, Springer, Berlin, 484-493.

Barthelmes, F., R. Dietrich and R. Lehmann (1991) Representation of the global gravity field modelling by overlaying of point masses on optimized positions based on recent spherical harmonics expansions. Paper presented to the XX General Assembly of the IUGG, Vienna, August.

Bronstein, I.N. and K.A. Semendyayev (1983) *Taschenbuch der Mathematik*. BSB R.G. Teubner Verlagsgesellschaft, Leipzig.

Denker, H., W. Torge, G. Wenzel, J. Ihde and U. Schirmer (1999) Investigation of different methods for the combination of gravity and GPS-levelling data. In: *Geodesy beyond 2000, the Challenges of the first Decade*, Springer, Berlin, 137-142.

Dentith, M.C., I. Bruner, A. Long, M.F. Middleton and J.Z. Scott (1993) Structure of the eastern margin of the Perth Basin, Western Australia. *Exploration Geophysics*, 24(3), 455-462.

Featherstone, W.E., A.H.W. Kearsley and J.R. Gilliland (1997) Data Preparations for a new Australian gravimetric geoid. *The Australian Surveyor*, 42(1), 33-44.

Featherstone, W.E. (1998) Do we need a Gravimetric Geoid or a Model of the Australian Height Datum to Transform GPS Heights in Australia?. *The Australian Surveyor*, 43(4), 273-280.

Featherstone, W.E. and M.P. Stewart (1998) Possible evidence for distortions in the Australian Height Datum in Western Australia. *Geomatics Research Australasia*, 68: 1-12.

Featherstone, W.E. (2000) Refinement of a gravimetric geoid using GPS and levelling data. *Journal of Surveying Engineering*, 126(2): 27-56.

Featherstone, W.E., J.F. Kirby, A.H.W. Kearsley, J.R. Gilliland, G.M. Johnston, J. Steed, R. Forsberg and M.G. Sideris (2001) The AUSGeoid98 geoid model of Australia: data treatment, computations and comparisons with GPS-levelling data. *Journal of Geodesy*, 75(5/6): 313-330.

Fraser, A.R., F.J. Moss and A. Turpie (1976) Reconnaissance gravity survey of Australia. *Geophysics*, 41, 1337-1345.

Friedlieb, O.J., W.E. Featherstone and M.C. Dentith (1997) A WGS84-AHD profile over the Darling Fault, Western Australia. *Geomatics Research Australasia*, 67, 1-17.

Heiskanen, W.A. and H. Moritz (1967) *Physical Geodesy*. Freeman, San Francisco, 364pp.

Ihde, J., U. Schirmer, F. Stefani and F. Töppe (1998) Geoid modelling with point masses. Proceedings of the Second Continental Workshop on the Geoid in Europe, Budapest, March, 199-204.

Johnston, G.M. and W.E. Featherstone (1998) AUSGeoid98 computation and validation: exposing the hidden dimension. Proceedings of the 39th Australian Surveyors Congress, Launceston, November, 105-116.

Kirby, J.F. and R. Forsberg (1998) A comparison of techniques for the integration of satellite altimeter and surface gravity data for geoid determination. In: *Geodesy on the Move: Gravity, Geoids, Geodynamics, and Antarctica*, Springer, Berlin, 207-212.

Kuhnert, F. (1976) *Pseudoinverse Matrizen und die Methode der Regularisierung*. BSB G.G. Teubner Verlagsgesellschaft, Leipzig.

Kupradze, V.D. and M.A. Aleksidze (1964) Metod funkcionalnych uravnenija dlja približennogo rešenija nekotorych graničnych zadač. *Žurn. vyčislit. matem. i matem. fiz.*, Moskva, 4, 4.

Lambeck, K. (1987) The Perth Basin: A possible framework for its formation and evolution. *Exploration Geophysics*, 18(3), 124-128.

Lehmann, R. (1993) The method of free-positioned point masses - geoid studies on the Gulf of Bothnia, *Bulletin Géodésique*, 67, 31-40.

Lehmann, R. (1994) Nonlinear gravity field inversion using point masses - diagnosing nonlinearity. In: *Geodesy and Physics of the Earth*, Springer, Berlin, 256-259.

Lemoine, F.G., S.C. Kenyon, J.K. Factor, R.G.Trimmer, N.K. Pavlis, D.S. Chinn, C.M.Cox, S.M. Klosko, S.B. Luthcke, M.H. Torrence, Y.M. Wang, R.G. Williamson, E.C. Pavlis, R.H. Rapp and T.R. Olson (1998) The development of the joint NASA GSFC and the National Imagery and Mapping Agency (NIMA) geopotential model EGM96, NASA/TP-1998-206861, National Aeronautics and Space Administration, USA.

Middleton, M.F., S.A. Wilde, B.A. Evans, A. Long and M. C. Dentith (1993) A preliminary interpretation of deep seismic reflection and other geophysical data from the Darling Fault Zone, Western Australia. *Exploration Geophysics*, 24(4): 711-718.

Roelse, A., H.W. Granger and J.W. Graham (1971) The adjustment of the Australian levelling survey - 1970-71. *Technical Report 12*, Division of National Mapping, Canberra.

Sandwell, D.T. and W.H.F. Smith (1997) Marine gravity anomaly from Geosat and ERS 1 satellite altimetry. *Journal of Geophysical Research*, 102(B5), 10039-10054.

Steed, J. and S. Holtznagel (1994) AHD Heights from GPS using AUSGeoid93. *The Australian Surveyor*, 39(1), 21-27.

Stewart, M.P., X.L. Ding, M. Tsakiri and W.E. Featherstone (1997) The 1996 STATEFIX Project. School of Surveying and Land Information, Curtin University of Technology, Perth, 47pp.

Stromeyer, D. and L. Ballani (1984) Uniqueness of the inverse gravimetric problem for point mass models. *manuscripta geodetica*, 9, 125-136.

Tziavos, I.N. and W.E. Featherstone (2001) First results of using digital density data in gravimetric geoid computation in Australia. In: Sideris, M.G. (ed) *Gravity, Geoid and Geodynamics 2000*, Springer, Berlin, 335-340.

Vening Meinesz, F.A. (1948) *Gravity expeditions at sea, 1923-1938*. Mulder, Delft.

Vermeer, M. (1995) Mass point geopotential modelling using fast spectral techniques; historical overview, toolbox description, numerical experiment. *manuscripta geodetica*, 20, 362-378.

Vermeer, M. (1998) Regularization Constraints in Mass Point Grids and their Relation to Gravity Field Stochastics. *Phys. Chem. Earth*, Vol. 23, No. 1, 13-18.

Weightman, J.A. (1965) Gravity, geodesy and artificial satellites, a unified analytical approach. Proceedings of the Second International Symposium on the Use of Artificial Satellites for Geodesy, Athens, 467-486.

Wellman, P., B.C. Barlow and A.S. Murray (1985) Gravity base station network values, *Report 261*. Bureau of Mineral Resources, Canberra, 38pp.